Mon. Not. R. Astron. Soc. **391,** 1650–1658 (2008) doi:10.1111/j.1365-2966.2008.14019.x

Multi-Conjugate Adaptive Optics VLT imaging of the distant old open cluster FSR 1415

Y. Momany,[1,2⋆] S. Ortolani,[3] C. Bonatto,[4] E. Bica[4] and B. Barbuy[5]

[1] *INAF, Osservatorio Astronomico di Padova, Vicolo dell'Osservatorio 5, I-35122 Padova, Italy*
[2] *European Southern Observatory, Alonso de Cordova 3107, Santiago, Chile*
[3] *Università di Padova, Dipartimento di Astronomia, Vicolo dell'Osservatorio 2, I-35122 Padova, Italy*
[4] *Universidade Federal do Rio Grande do Sul, Departamento de Astronomia CP 15051, RS, Porto Alegre 91501-970, Brazil*
[5] *Universidade de São Paulo, IAG, Rua do Matão 1226, Cidade Universitária, São Paulo 05508-900, Brazil*

Accepted 2008 September 29. Received 2008 September 28; in original form 2008 August 16

ABSTRACT

We employ the recently installed near-infrared Multi-Conjugate Adaptive Optics demonstrator (MAD) to determine the basic properties of a newly identified, old and distant, Galactic open cluster (FSR 1415). The MAD facility remarkably approaches the diffraction limit, reaching a resolution of 0.07 arcsec (in K), that is also uniform in a field of ∼1.8 arcmin in diameter. The MAD facility provides photometry that is 50 per cent complete at $K \sim 19$. This corresponds to about 2.5 mag below the cluster main-sequence turn-off. This high-quality data set allows us to derive an accurate heliocentric distance of 8.6 kpc, a metallicity close to solar and an age of ∼2.5 Gyr. On the other hand, the deepness of the data allows us to reconstruct (completeness-corrected) mass functions (MFs) indicating a relatively massive cluster, with a flat core MF. The Very Large Telescope/MAD capabilities will therefore provide fundamental data for identifying/analysing other faint and distant open clusters in the Galaxy III and IV quadrants.

Key words: instrumentation: adaptive optics – techniques: photometric – stars: Population II – open clusters and associations: individual: FSR 1415 – infrared: stars.

1 INTRODUCTION

Open clusters are continuously affected by dynamical processes such as: (i) mass loss, linked to stellar evolution, mass segregation and evaporation; (ii) tidal interactions with the Galactic disc and bulge and (iii) collisions with giant molecular clouds. These processes combined tend to accelerate the internal dynamical evolution which, as the cluster ages, results in significant changes in the cluster structure and mass function (MF) (Bonatto & Bica 2007b, and references therein). Eventually, the majority of the open clusters will be dispersed in the Galactic stellar field or become poorly populated remnants (Pavani & Bica 2007, and references therein). In fact, open clusters older than ∼1 Gyr are found preferentially near the solar circle and in the outer Galaxy (e.g. Friel 1995; Bonatto et al. 2006b), where the frequency of dynamical interactions with giant molecular clouds and the disc is low (e.g. Upgren, Mesrobian & Kerridge 1972; Salaris, Weiss & Percival 2004).

As a reflex of the above scenario, less than ∼18 per cent of the open clusters listed in WEBDA are older than 1 Gyr, with most of them located outside the solar circle (see e.g. fig. 1 of Bonatto & Bica 2007b). Granted the above aspects, the discovery and derivation of astrophysical parameters of old open clusters are expected to result in a better understanding of the dynamical processes that affect star clusters, with reflexes on star formation and evolution processes, dynamics of N-body systems and the geometry of the Galaxy, among others.

In this framework, the construction of an old (≥1 Gyr), distant and complete open cluster sample acquires particular importance. An effort in this direction is the new catalogue of 1021 star cluster candidates that was recently presented by Froebrich et al. (2007a, hereafter FSR objects). It spans all Galactic longitudes (for $|b| < 20^{\circ}$) and is based on an overdensity automated search algorithm applied to the 2MASS[1] data base. The examination of this catalogue has surprisingly allowed the detection of new globular clusters (FSR 1735, FSR 1767, Bonatto et al. 2007; Froebrich, Meusinger & Scholz 2007b) and a number of old open clusters (e.g. FSR 1744, FSR 31, FSR 89; Bonatto & Bica 2007a). We have examined many cluster candidates from this catalogue and verified that several of these must have the turn-off (TO) much below the 2MASS limit. Thus, and for a few cases, the photometry provided by a 4-m-class telescope was still not deep enough (Froebrich, Meusinger & Scholz

⋆E-mail: yazan.almomany@oapd.inaf.it

[1] The Two-Micron All-Sky Survey, available at www.ipac.caltech.edu/2mass/releases/allsky/.

2007b; Froebrich, Meusinger & Davis 2008) and; consequently, 8-m-class telescopes [provided that adaptive optics (AO) is available] were needed.

The recent availability of a Multi-Conjugate Adaptive Optics Demonstrator (MAD) at the Very Large Telescope (VLT) UT3-Melipal and the public call for Science Verification encouraged us to propose *JK* observations of the faint cluster FSR 1415. Indeed, the inspection of the 2MASS colour–magnitude diagrams (CMDs) indicated the presence of either (i) a rich red clump (RC) or (ii) a red horizontal branch. Disentangling between these two, similar, features allows one to infer the detection of a distant old open cluster or a globular cluster, respectively. The results presented in this paper (Section 2) unequivocally point towards the detection of an old open cluster. We stress that there are very few photometric studies of Galactic star clusters with standard AO (Trumpler 14; Ascenso et al. 2007) or with Multi-conjugate Adaptive Optics (Trapezium by Bouy et al. 2008, see also the case of the UKS2323-326 dwarf galaxy by Gullieuszik et al. 2008). FSR 1415 is a low-latitude target projected almost orthogonally to the Galactic anticentre direction ($\ell = 263\overset{\circ}{.}74$, $b = -1\overset{\circ}{.}81$). The J2000 equatorial coordinates are $(\alpha, \delta) = (8\overset{h}{.}40\overset{m}{.}24\overset{s}{}, -44\overset{\circ}{.}43\overset{m}{.}05\overset{s}{})$.

Although the present study addresses a single open cluster, it lays the basis for the identification of a complete sample of old open clusters in the IV Galaxy quadrant, known for a dearth of distant and old clusters. Ultimately, a complete sample will be useful for understanding the evolution of the disc, in particular that concerning radial gradients and age–metallicity relations (Friel 1995; Rocha-Pinto et al. 2006; Maciel, Quireza & Costa 2007). In Section 2, we describe the instrument and observing procedures. In Section 3, we present the photometry and derive cluster parameters, including a study of the radial structure. In Section 4, we discuss the results of FSR 1415 in the context of other old open clusters and the properties of the disc. In Section 5, conclusions and perspective work on clusters with AO are presented.

2 OBSERVATIONS

MAD was developed by the European Southern Observatory (ESO) Adaptive Optics Department to be used as a visitor instrument at Melipal in view of an application to ELT. It was installed at the visitor Nasmyth focus and introduces the concept of multiple reference stars for layer-oriented AO corrections. This allows a much wider and more uniform corrected field of view, providing larger average Strehl ratios and making the system a powerful diffraction limit imager. This is particularly important in crowded fields where the photometric accuracy is needed. For more details see http://www.eso.org/projects/aot/mad/ and Marchetti et al. (2007). Indeed, the on-sky MAD commissioning of an ωCen field showed an enormous gain in angular resolution and light concentration such that very faint stars ($K \sim 20.5$) were easily distinguished (at a 3σ level) in just 600 s exposures. In 2007 October, we answered a call for science demonstration of MAD, and among other applications (see http://www.eso.org/sci/activities/vltsv/mad/), we were granted a total of two hours aimed at deriving the main properties of a distant cluster candidate (FSR 1415).

Within the field of view of the instrument, three reference bright stars were selected to ensure the optics correction. These stars had *V* magnitudes that ranged between 12.24 and 13.6, according to their GSC2.2 magnitude system. While the site seeing during the observations was $\approx$0.8 arcsec, a diffraction limit in *K* of 0.07 arcsec was reached. Table 1 displays the logbook of the *J* and K_s (for brevity we use *K*) observations. The MAD infrared scientific imaging camera

Table 1. Log of the MAD observations obtained on 2008 January 13.

Filter	FWHM (arcsec)	airmass	DIT (s)	NDIT
K	0.085	1.145	10	27
K	0.073	1.137	10	27
K	0.073	1.129	10	27
K	0.074	1.122	10	27
J	0.145	1.248	10	27
J	0.101	1.234	10	27
J	0.176	1.221	10	27
J	0.195	1.209	10	27

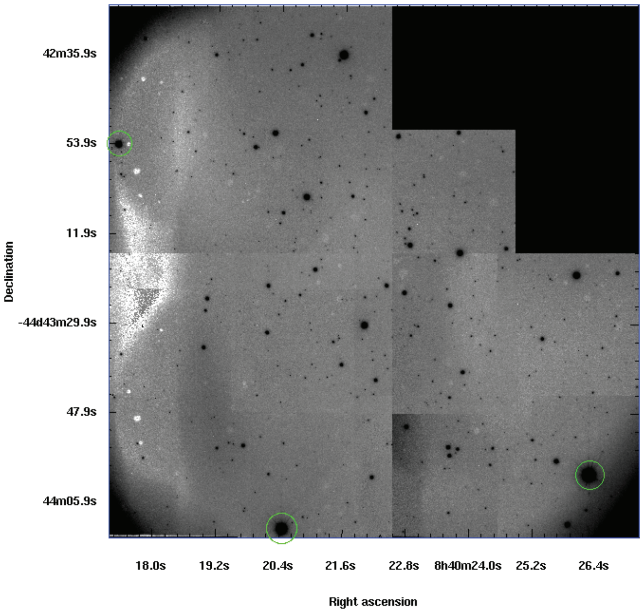

Figure 1. The MAD mosaic of the eight *J*- and *k*-dithered images of FSR 1415: east is to the right and north to the top. The overall circular field of view is $\sim$1.8 $\times$ 1.8 arcmin. The irregular shape of the mosaic is due to the lacking of a fifth dithered image. Border vignetting and other features (due to the movable scanning table) are unavoidable.

is based on a 2048 $\times$ 2048 pixel HAWAII-2 infrared detector with a pixel scale of 0.028 arcsec.

Given that the Detector Integration Time (DIT) is the amount of time during which the signal is integrated on to the detector diodes, while NDIT is the number of detector integrations that are obtained and averaged together, it follows that the total exposure time of a single raw image is simply NDIT$\times$DIT. In our case, we obtained four dithered images in each filter, where DIT was fixed to 10 s and NDIT to 27 s. Thus, the total exposure time is 1080 s (18 min) in *J* and *K*. The images were dark and sky-subtracted and then flat-fielded following the standard near-infrared recipes (see e.g. Dutra et al 2003; Momany et al. 2003), all performed under the IRAF environment.

Fig. 1 shows the mosaic of all eight *J* and *K* images as constructed by DAOPHOT/MONTAGE2 task. Fig. 2 shows the full width at half-maximum (FWHM) map with an overall regular distribution across the entire field of view with values ranging between $\sim$2.5 (0.07 arcsec) and $\sim$4.5 (0.13 arscsec), where the upper limit is mostly due to the fitting process in the border zones with scarce

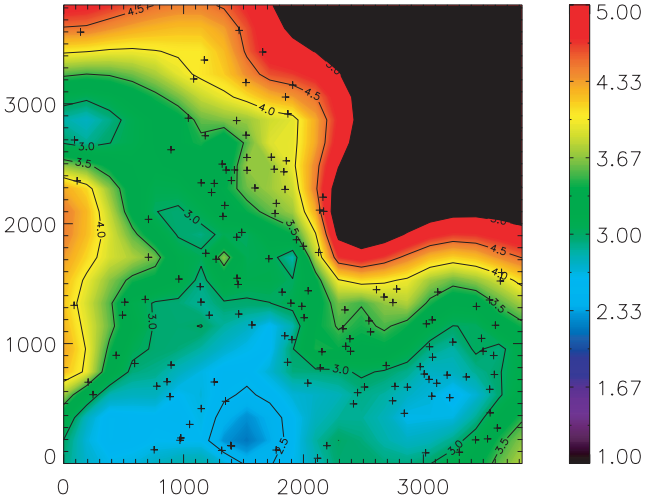

Figure 2. The *X* and *Y* FWHM map (in pixels) of the eight *J* and *K* mosaicked images. East is to the right and north to the top. Crosses show the stars identified and used in the FWHM computation (1 pixel is 0.028 arcsec).

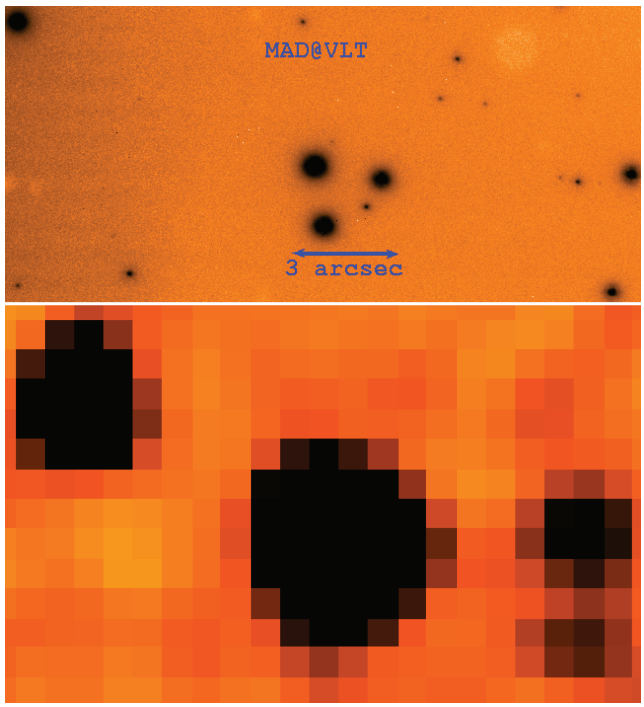

Figure 3. The resolution supremacy of the MAD *K* image as compared to the 2MASS. The quadruple MAD stars with *K* magnitudes of 13.536, 13.868, 14.391 and 17.155 are identified as one single star ($K = 12.853 \pm 0.040$ and $J = 13.536 \pm 0.038$) in the 2MASS catalogue.

stellar population. The superb VLT/MAD resolution is illustrated in Fig. 3, in a comparison with the 2MASS photometry.

2.1 Photometric reduction

Stellar photometry was obtained by point spread function (PSF) fitting using the tested DAOPHOT II/ALLFRAME (Stetson 1994) package. ALLFRAME combines PSF photometry carried out on the individual images and allows the creation of a master list by combining images from different filters, thereby pushing the detection limit to

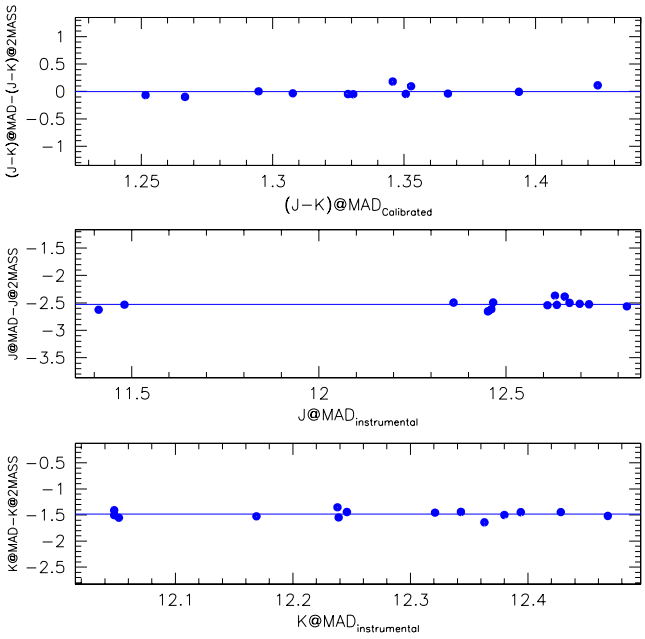

Figure 4. The lower and middle panels display a comparison of the *J* and *K* MAD instrumental photometry with 2MASS magnitude. Upper panel shows the $(J - K)$ colour difference among the two photometric systems once the offsets have been applied to the MAD data.

fainter magnitudes. Once the FIND and PHOT tasks were performed, we searched for isolated stars to build the PSF for each single image. The final PSF was generated with a PENNY function that had a quadratic dependence on position in the frame.

2.2 Calibration

Calibration of the *J* and *K* data has been made possible by direct comparison of the brightest MAD non-saturated stars with their 2MASS photometry. Fig. 4 shows the *J* and *K* magnitude differences between our MAD instrumental photometry and that from 2MASS. In particular, the majority of the stars in common are the RC stars. From these stars we estimate a mean offset of $\Delta J_{\rm J@MAD-J@2MASS} = -2.516 \pm 0.081$ and $\Delta K_{\rm K@MAD-K@2MASS} = -1.477 \pm 0.074$. The upper panel shows a comparison between the MAD and 2MASS photometry once the above offsets have been applied to the MAD data.

2.3 Photometric errors and completeness

Photometric errors and completeness were estimated from the artificial stars experiments following procedures similar to those in Momany et al. (2002, 2005). More than 2300 artificial stars were added to the single images, and these were placed in a suitable pattern of triangular meshes to avoid self-crowding and not closer than 40 pixels (1.1 arcsec). In particular, the distribution of the *J* and *K* magnitudes was not casual, and these were simulated in a way to reproduce the cluster main-sequence (MS) and red giant branch (RGB) loci. The images with the artificial stars added were then reprocessed in the same manner as the original images. The results for photometric completeness and errors are presented in Figs 5 and 6.

Fig. 5 compares the nominal DAOPHOT II photometric errors (black dots) with those derived from the comparison between the magnitude of input simulated stars and the retrieved magnitudes. The

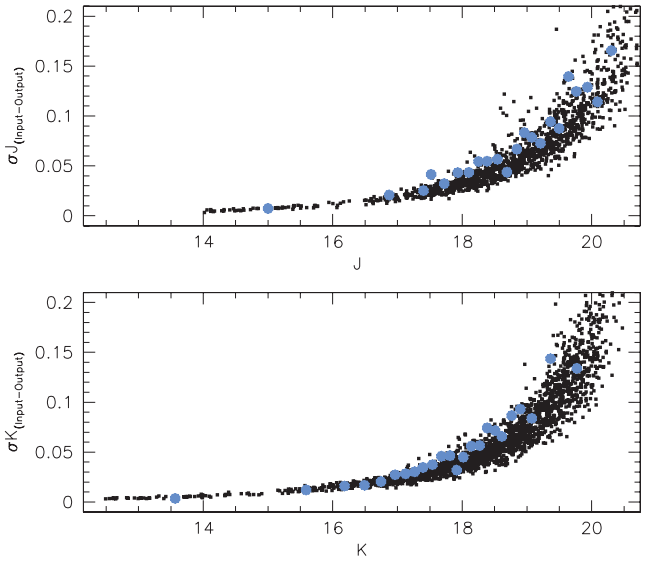

Figure 5. The *J* and *K* photometric errors (black dots) as provided by the DAOPHOT/ALLFRAME reduction. Light-starred symbols display the estimated photometric errors as derived from the artificial stars experiment.

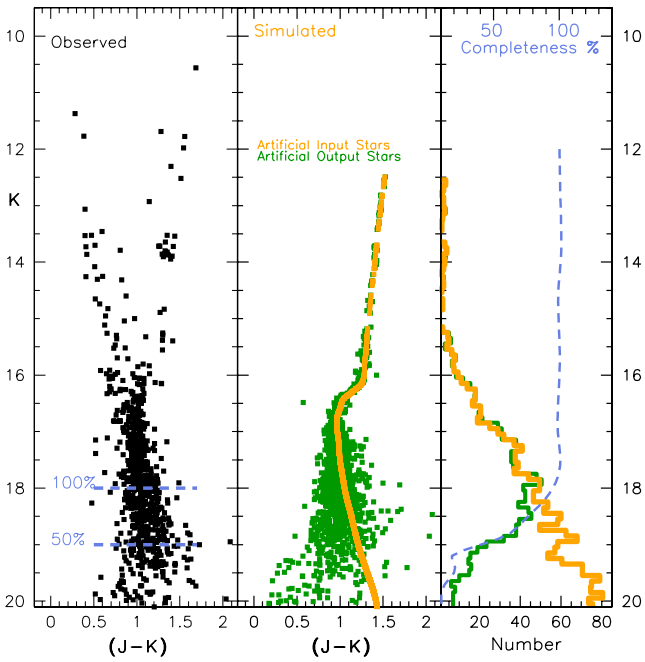

Figure 6. Results of the artificial stars experiments. Left-hand panel shows the observed CMD while the middle panel displays the input and output CMD of the simulated stars. The right-hand panel compares the luminosity function of the input/output artificial stars, whereas the light-dashed line shows the computed *K* completeness level.

light-starred symbols report the mean photometric errors where the binning is that of a fixed number of 50 artificial stars. The comparison shows an overall consistency between the two derived errors, although there is a hint of a slightly higher photometric error as derived from the artificial stars experiments. On the other hand, Fig. 6 summarizes the estimated photometric completeness of our data. The left-hand panel of Fig. 6 shows the observed colour–magnitude diagram (CMD), whereas the middle panel displays the colour–magnitude distribution of the input ∼2300 artificial stars (orange dots obtained reproducing the MS and RGB fiducial line of the cluster) and the retrieved artificial stars (green dots). The distribution of the retrieved artificial stars reflects the increasing level of photometric errors and the lower completeness levels towards fainter magnitudes. The right-hand panel compares the luminosity distribution of the input and output stars, whereas the light-dashed line computes the output/input stars ratio (reflecting the completeness of the data). In calculating this ratio, only stars recovered in both the *J* and *K* images are considered. Thus, Fig. 6 shows that our CMDs are basically complete down to $K \sim 18.0$, reaching a 50 per cent completeness level around $K \sim 19.0$. For a mean $(J - K)$ colour of ∼1.0, we report the *K* completeness levels in Table 2.

Table 2. *K*-completeness levels as derived from the artificial stars experiments for an average $(J - K) \sim 1.0$ of the input stars.

K mag	Comp. (per cent)	*K* mag	Comp. (per cent)
12.0	100	18.2	89
12.5	100	18.4	80
13.0	100	18.6	72
13.5	100	18.8	62
14.0	100	19.0	40
14.5	100	19.2	18
15.0	100	19.4	20
15.5	100	19.6	16
16.0	100	19.8	11
16.5	99	20.0	10
17.0	98	20.2	6
17.5	98	20.4	0
18.0	95	–	–

3 ANALYSIS OF THE PHOTOMETRY

The left-hand panel of Fig. 7 displays our VLT/MAD CMD of the entire FSR 1415 field (∼1.8 × 1.8 arcmins). Superimposed in light open circles are 2MASS stars falling in the same field. The CMD contains obvious open cluster features, i.e. the RGB, the RC, the main-sequence turn-off (MSTO) and the expected cluster blue stragglers (BS) population. The latter population is confused by the presence of nearby Galactic disc MS stars (the oblique sequence extending to $K \sim 11.0$). It remains, however, that the two prominent open cluster features are the RC and the MSTO. Indeed, despite the relatively small MAD field of view, we sample to about 10 RC stars. The average location of these RC stars is at $K = 13.82 \pm 0.03$ and $(J - K) = 1.34 \pm 0.03$. On the other hand, the MSTO is located at $K = 16.65 \pm 0.05$. Thus, the difference between the MSTO and RC is $\Delta K_{\rm RC}^{\rm TO} = 2.83 \pm 0.06$, typical of old open clusters.

Although no control field has been observed, the SKY single images (usually medianed to eliminate stars) can be treated just as a scientific image, and reduced similarly. This should provide us with an idea of the contaminant field population around FSR 1415. We stress the fact, however, that these SKY images are not obtained with a closed AO loop, thus the resultant CMD is clearly shallower. At ∼8 arcmin from the FSR 1415, one easily identifies a complete absence of RC stars. This is also confirmed by the 2MASS photometry in the same area, and therefore the identification of a genuine open cluster (left-hand panel) is further confirmed.

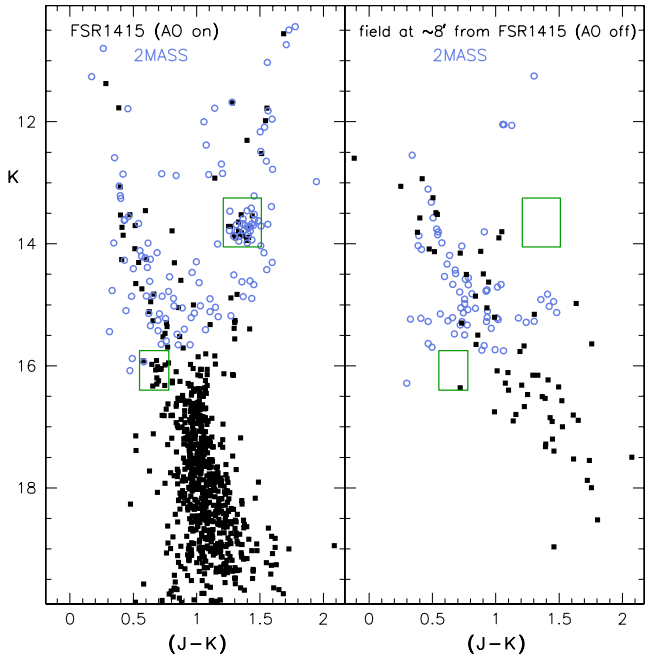

Figure 7. Left-hand panel displays the MAD CMDs of the FSR 1415 field (AO switched on) superimposed on the 2MASS photometry (in the same area). Right-hand panel displays the diagrams of the SKY field (AO switched off) at 8.0 arcmin from FSR 1415. The boxes in both panels highlight the difference in RC and BS stars.

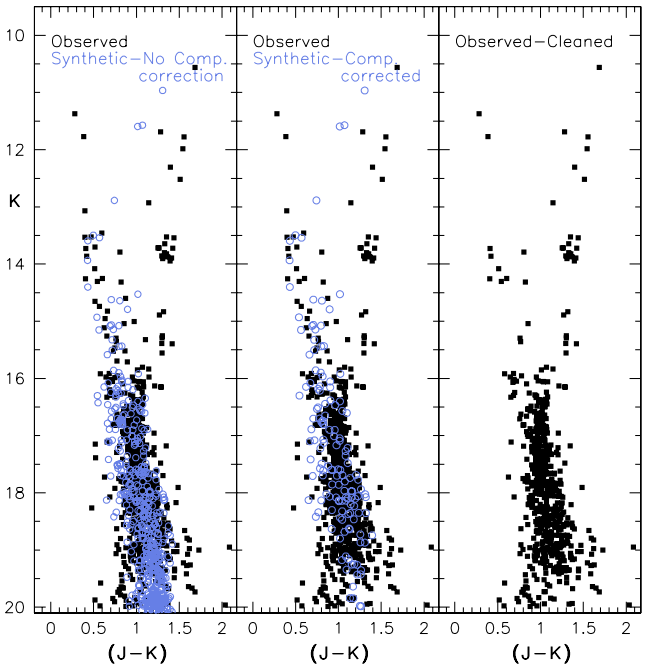

Figure 8. Left-hand panel displays the observed MAD CMD along with a synthetic CMD in the FSR 1415 line of sight. The middle panel shows the same diagrams after degrading the synthetic CMD with the estimated photometric completeness of our MAD field. Right-hand panel displays the 'cleaned' FSR 1415 diagram after subtracting the field contribution.

3.1 A blue stragglers population?

To confirm the possible presence of a BS population in FSR 1415, one needs to account for the disc population around the cluster. In the absence of a deep CMD of the FSR 1415 surrounding environment, we attempt to solve this issue by the use of synthetic diagrams based on the models of the Galaxy. The Besançon (Robin et al. 2003) online simulator provides synthetic CMDs in specific line of sights for a given area. Applying the cluster Galactic coordinates and field of view, in Fig. 8, we overplot the synthetic Galactic CMD upon the observed FSR 1415 CMD.

A glance at the left-hand panel of Fig. 8 shows an excellent agreement of the simulated Galactic population in this line of sight and the observed CMD. Indeed, at latitudes of $b = -1.^{\circ}81$ one expects to detect only young stellar disc populations, and this agrees with the oblique young MS extending to $K \sim 12.0$. There is, however, a significant difference in the star counts of the synthetic MS and that expected in our observed CMD. This is due to the fact that the synthetic CMDs do not 'suffer' photometric completeness effects. Employing our artificial stars experiments and the resultant photometric completeness curve, in the middle panel we 'correct' the star counts of the synthetic MS for photometric completeness. The middle panel shows that a remnant Galactic MS population remains present and must be accounted for in any star count's analysis of FSR 1415 populations. Dividing the CMD in cells of 0.5 and 0.4 in magnitudes K and $(J - K)$, respectively, we derive the number of Milky Way MS stars and randomly subtract this contribution from the observed MAD diagram.

The right-hand panel of Fig. 8 presents the result of this statistical decontamination process. Clearly, there remains a clump of MS stars at $K \sim 14.0$ and $(J - K) \sim 0.5$, and this can be explained as due to the small number statistics involved in the simulation. Nevertheless, the 'cleaned' diagram now shows a clear bifurcation around the cluster MSTO, indicating the probable detection of the BS sequence.

To ascertain whether the FSR 1415 BS candidates are true cluster members, we estimate the parameter $F_{\rm RC}^{\rm BSS} = \log(N_{\rm BS}/N_{\rm RC})$ (see de Marchi et al. 2006) and check if this frequency is compatible with that in other open clusters. We count 14 BS stars *versus* 10 RC stars, providing an $F_{\rm RC}^{\rm BSS}$ of 0.146. This is fully compatible with the values for other open clusters (0.2 ± 0.2), indicating that we have probably detected a genuine BS population in FSR 1415. Interestingly, fig. 2 of Momany et al. (2007) compares the $F_{\rm RC}^{\rm BSS}$ in different environment (spanning from open and globular clusters to nearby dwarf galaxies) and shows that open clusters and the lowest luminosity dwarf galaxies (e.g. the Bootes dwarf at $M_V = -5.5$) share the same BS frequency. This has been interpreted as the consequence of the presence of an observational upper limit to the frequency production of primordial BS in low-density stellar systems.

3.2 Age, metallicity and distance

To enhance the signature of the cluster population with respect to the foreground disc contamination, in Fig. 9 we display the CMDs of FSR 1415 extracted within a radius of $r \leq 0.5$ arcmin. Despite the smaller field of view, the extracted CMDs still show a well-populated RC and MSTO, ideal features for the derivation of the cluster age. As a first approach, we assume that the four stars at $J \approx 17$ are cluster subgiants. We note indeed that these stars survive our decontamination process (see the right-hand panel of Fig 8). This granted, and following various tentatives, in Fig. 9, we show our best isochrone match to the CMD. This has been achieved using isochrones from the Padova library (Girardi et al. 2002) for an age of 2 Gyr, metallicity $Z = 0.019$, a reddening of $E(J - K) = 0.72$

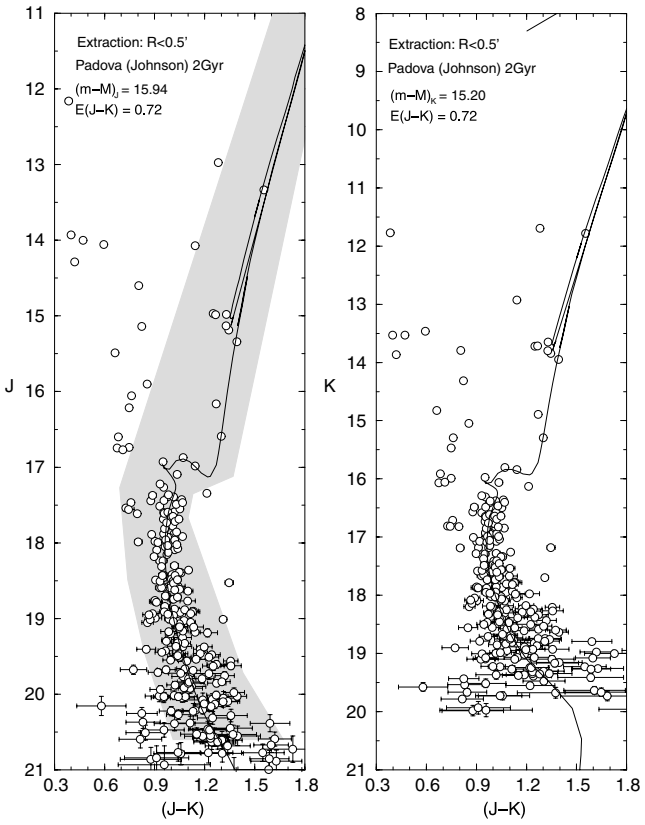

Figure 9. Observed J and K *versus* $(J-K)$ CMDs of FSR 1415 within $r < 0.5$ arcmin from the cluster centre. Superimposed is the best fit of a theoretical 2 Gyr solar metallicity isochrone from the Padova library. The shaded area highlights the colour–magnitude filter used in the derivation of the mass function.

and an apparent distance modulus $(m-M)_K = 15.20$. With respect to the observed FSR 1415 RGB and clump, we note that isochrones more metal rich than the solar are, in general, redder. On the other hand, isochrones with metallicities less than solar provide a poorer match of the cluster MSTO. Fixing a solar metallicity and allowing for age variations, we conclude that the cluster age is constrained at 2.5 ± 0.7 Gyr. For infrared ratios between absorption and colours, we use the results from Dutra, Santiago & Bica (2002), and references therein. The derived $E(J-K)$ value thus converts to $E\,(B-V) = 1.47$ or $A_V = 4.56$. From the isochrone fit we derive that the heliocentric distance of FSR 1415 is $d_\odot = 8.59$ kpc.

It would be of great interest to have a spectroscopic determination of metallicity of FSR 1415, such as has been done in recent years by e.g. Friel et al. (2002), Yong, Carney & Teixeira de Almeida (2005) and Bragaglia et al. (2008). This will ultimately reduce the current age uncertainty. Table 3 summarizes the derived cluster parameters and errors.

3.3 Location in the Galaxy

In the derivation of the spatial Galactic coordinates of FSR 1415, one needs to assume the Sun's distance from the Galactic Centre ($R_\odot$). Interestingly, the last few years have witnessed a clear trend towards shorter distance scales with respect to the nominal value of $R_\odot = 8.0$ kpc (see Reid 1993). Indeed, Eisenhauer et al. (2005) derive $R_\odot = 7.6 \pm 0.3$ kpc, whereas Nishiyama et al. (2006) find $R_\odot = 7.5 \pm 0.35$ kpc and Bica et al. (2006) report $R_\odot = 7.2 \pm 0.3$ kpc. The

Table 3. Parameters of FSR 1415, as derived in this paper. We assume $R_\odot = 7.2$ kpc.

Parameters	Values	Parameters	Values
$(m-M)_K$	15.20 ± 0.10	$d_\odot$	8.59 ± 0.45 kpc
$(m-M)_J$	15.94 ± 0.10	R_{GC}	11.8 ± 0.5 kpc
$E(J-K)$	0.72 ± 0.02	X_{GC}	-8.2 ± 0.1 kpc
$E(J-H)$	0.46 ± 0.02	Y_{GC}	-8.5 ± 0.5 kpc
$E\,(B-V)$	1.47 ± 0.06	Z_{GC}	-0.3 ± 0.1 kpc
A_V	4.56 ± 0.11	$\mathrm{Mass_{Obs.}}$	390 $M_\odot$
Age	2.5 ± 0.7 Gyr	$\mathrm{Mass_{extrap.}}$	$2-3 \times 10^4$ $M_\odot$
[Fe/H]	solar	R_c	2.6 ± 0.6 pc
$(m-M)_\circ$	14.67 ± 0.11	R_t	35 ± 8 pc

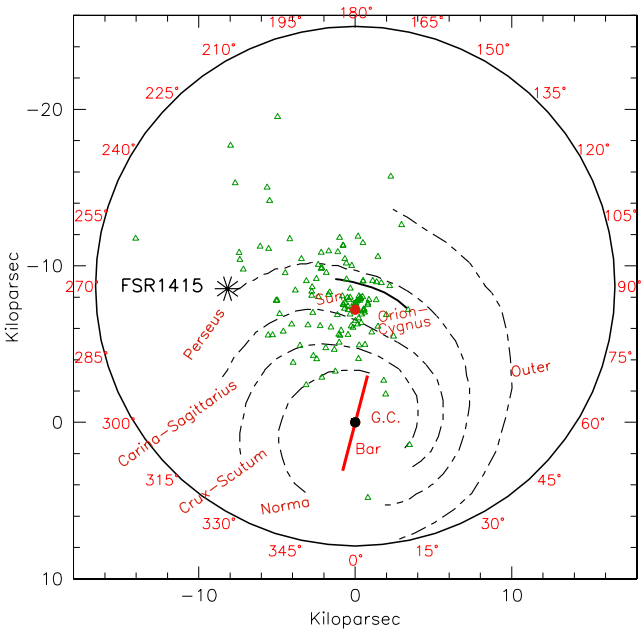

Figure 10. A schematic view of the Milky Way as seen from its North Pole showing the four spiral arms, the Galactic Centre and the Sun's position (with $R_\odot = 7.2 \pm 0.3$ kpc). Also plotted are a WEBDA open cluster compilation (limited to an age of $\geq$1 Gyr) and the position of FSR 1415 as derived in this paper.

latter value is based on an updated globular cluster compilation and is adopted throughout this paper. We note, however, that recently Groenewegen, Udalski & Bono (2008), with Population II Cepheids and RR Lyrae stars, report a longer distance ($R_\odot = 7.94 \pm 0.37$ kpc). In conclusion, and assuming $R_\odot = 7.2 \pm 0.3$ kpc, we derive that the Galactocentric distance of FSR 1415 is $R_{GC} = 11.81 \pm 0.33$ kpc, which puts it $\approx$4.6 kpc outside the solar circle.

To place FSR 1415 in a bigger framework, we display in Fig. 10 a schematic view of the Milky Way Galaxy (from Drimmel & Spergel 2001, see also Vallée 2008) in which its major features, spiral arms and bar are outlined. Superimposed (as open triangles) we show the positions of 125 known old ($\geq$1 Gyr) open clusters, taken from the WEBDA data base (Mermilliod 1996).[2] Their spatial distribution shows a clear detection 'bias', in the sense of a concentration towards the Sun and the solar circle. In this context, FSR 1415 stands

[2] The Galactocentric coordinates of the WEBDA open cluster sample have been calculated assuming $d_\odot = 7.2$ kpc as derived in Bica et al. (2006).

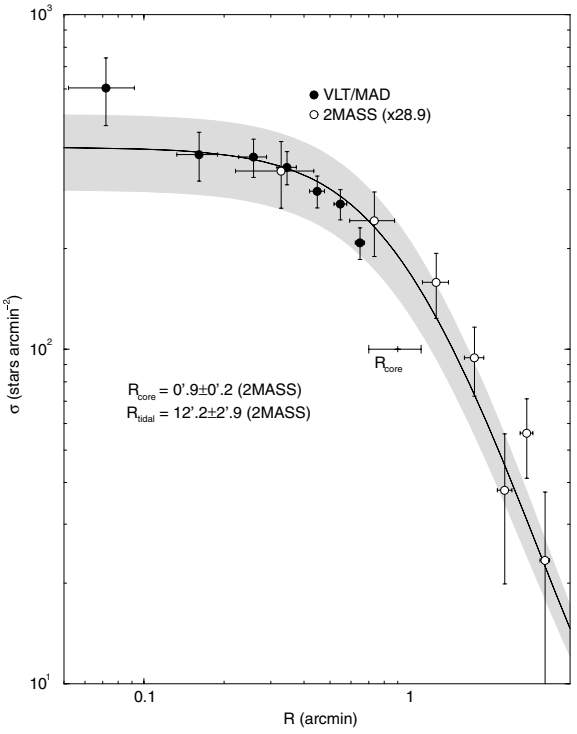

Figure 11. VLT/2MASS merged stellar density profile as a function of the projected distance to cluster centre. The observed set of stars was employed. A three-parameter King profile fit is superimposed (solid line). Shaded area corresponds to the 1σ fit uncertainties. The core and tidal radii have been derived from the 2MASS data.

out as a distant cluster in quadrant III of the Galaxy, located at $R_{GC} = 11.81$ kpc from the Galactic Centre.[3] Fig. 10 shows that there are a handful of old open clusters in this direction, and that more old clusters await to be identified in quadrant IV. Besides their age, another interesting aspect of old clusters such as FSR 1415 is their identification as outer disc clusters. Indeed, the determination of their metallicity will be crucial in extending the analysis of reported metallicity gradients far to the Milky Way outskirts.

3.4 Structure

Structural parameters of FSR 1415 were derived from the cluster stellar radial density profile (RDP), which consists of the projected number density of stars around the cluster centre. The RDP of FSR 1415 was built by merging the observed VLT photometry in the inner region and the 2MASS data in the outer part (e.g. Bonatto & Bica 2007a). The field background was obtained from the 2MASS data and subtracted. The background-subtracted 2MASS profile has been scaled to match the VLT one by multiplying the 2MASS RDP by 28.9. The VLT profiles of FSR 1415 are limited to $K = 19.0$, which corresponds to the stellar mass of $\approx 0.93\,M_\odot$. We employ the observed photometry because the artificial stars do not take into account dynamical effects. The VLT/MAD central surface density is a factor of $\approx$30 higher than that of the 2MASS profile, which is consistent with the $\approx$4 mag deeper VLT photometry.

In Fig. 11, we show the merged VLT/2MASS density profile. Star clusters have RDPs that can be described by some well-defined analytical profile. The most widely used are the single mass, modified isothermal sphere of King (1966), the modified isothermal sphere of Wilson (1975) and the power law with a core of Elson et al. (1987).

These functions are characterized by different sets of parameters that describe the cluster structure. Since we are working with a RDP built from different photometric sets and that our goal here is basically to derive reliable structural parameters for FSR 1415, we fit the RDP with the analytical three-parameter function $\sigma(R) = \sigma_0[\frac{1}{\sqrt{1+(R/R_c)^2}} - \frac{1}{\sqrt{1+(R_t/R_c)^2}}]^2$, where σ_0 is the central number density of stars, and R_c and R_t are the core and tidal radii, respectively. This function is similar to that introduced by King (1962) to describe the surface brightness profiles in the central parts of globular clusters. Moreover, as discussed in Bonatto & Bica (2008a) and Bonatto & Bica (2008b), RDPs built with photometry as deep as in the present case produce very robust structural parameters when fitted with the three-parameter King-like function. In such cases, RDPs yield similar parameters as with surface brightness profiles.

The results of the fit parameters indicate a core radius of $R_c = 0.9 \pm 0.2$ arcmin (corresponding to 2.6 ± 0.6 pc) and a tidal radius of $R_t = 12.2 \pm 2.9$ arcmin (or 35 ± 8 pc). Thus, most of the VLT/MAD observations are restricted to within the core. The resulting central density is $\sigma = 462 \pm 118$ stars arcmin^{-2} (55 ± 14 stars pc^{-2}). With respect to the three-parameter King fit, we note that the innermost RDP point at $R \sim 0.07$ arcmin ($\sim$0.2 pc) shows a marginal 1σ stellar density excess. Although marginal in the case of FSR 1415, such a feature is characteristic of post-core-collapse globular clusters (Trager, King & Djorgovski 1995), and may indicate an advanced dynamical evolution state in the core of FSR 1415 (see Section 3.5). The presence of post-core-collapse features in RDPs of open clusters has been previously detected, for instance, in the $\sim$1 Gyr cluster NGC 3960 (Bonatto & Bica 2006).

3.5 Luminosity and mass functions

The observed luminosity and mass functions (LF and MF,respectively) for the J and K bands were built using the parameters in Table 2. We applied a colour–magnitude filter to the observed photometry (Fig. 9) to minimize contamination (e.g. Bonatto & Bica 2007a).

Fig. 12 shows the LFs measured in the K band for the regions $0.0 - 0.3$, $0.3 - 0.6$ and $0.0 - 0.6$ arcmin. It is interesting to note that these LFs correspond to spatial regions contained within the core (Section 3.4), and differences among them might be related to the dynamical effects inside the core. The actual number of member (i.e. decontaminated) stars included in the computation of the $R < 0.6$ arcmin LF is 321, 307 of which are MS stars, while the remaining are evolved. Granted the isochrone solution derived in Section 3.2, we estimate (for the observed magnitude range) that the cluster stellar mass amounts to $390\,M_\odot$ ($367\,M_\odot$ as MS and $23\,M_\odot$ as evolved stars).

Since completeness is an important issue (Section 2.3) for fainter stars, we show the completeness levels for selected four K magnitudes. Besides the observed LFs, we also show the corresponding completeness-corrected ones. The observed LFs do not appear to change significantly within the core. The same applies to the completeness-corrected LFs.

Mass functions for the same spatial regions as the LFs were constructed by combining the two J and K independent MFs (see e.g. Bonatto & Bica 2005). The MFs were computed for the mass range $m > 0.87\,M_\odot$, corresponding to $J \lesssim 20.2$ and $K \lesssim 19.3$.

[3] With $R_\odot = 8.0$ instead of 7.2, the resultant distance from the Galactic Centre would be 12.18 ± 0.34 kpc.

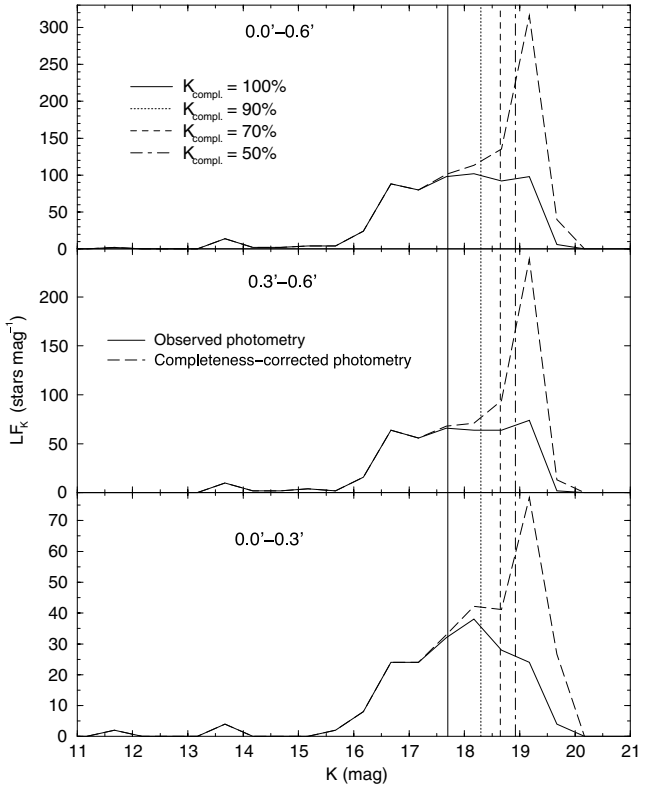

Figure 12. Luminosity functions in the K band for an inner (bottom panel), intermediate (middle panel) and wide (top panel) regions. These regions are inside the core. Completeness values for selected magnitudes are shown as vertical lines. LFs with the observed (heavy-solid line) and completeness-corrected (heavy-dashed line) photometry are shown for comparison.

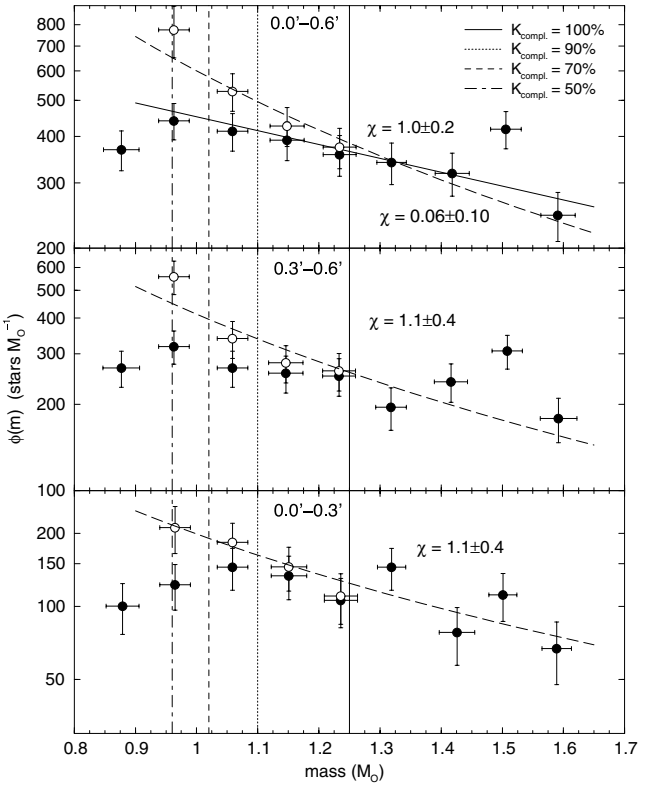

Figure 13. Mass functions for the total (top panel), intermediate (middle) and inner (bottom) regions. The observed (filled symbols) and completeness-corrected MFs (empty) are used. The mass values where the 100 per cent, 90 per cent, 70 per cent and 50 per cent K completeness occur are indicated (vertical lines). Fits of $\phi(m) \propto m^{-(1+\chi)}$ are also shown.

These are shown in Fig. 13, where the relatively small MF error bars reflect the statistical significance of the star counts. At first sight, the observed MFs are flat, showing small differences between the two innermost regions. There is, however, an important drop towards the low-mass stars. Although, in principle, this might be related to mass segregation inside the core, nevertheless, crowding and completeness should be taken into account before a similar conclusion can be established. To this purpose, we also built the completeness-corrected MFs (as done for the LFs; Fig. 12). As expected, a significant difference between the observed and the completeness-corrected MFs is observed for masses below 1.1 $M_\odot$.

For a better description of the cluster MFs, we fit these with the function $\phi(m) \propto m^{-(1+\chi)}$, carried out for masses higher than $m > 0.96\,M_\odot$ ($J \simeq 19.8$, $K \simeq 18.9$). The lowest mass point, at $\approx 0.88\,M_\odot$, is exceedingly affected by completeness. The fit to the observed 0.0−0.6 arcmin MF (top panel) provides a slope of $\chi = 0.06 \pm 0.10$, significantly flatter than the $\chi = 1.35$ of Salpeter (1955) initial mass function (IMF). However, when the same fit is applied to the completeness-corrected MF, the resultant slope increases to $\chi = 1.0 \pm 0.2$, thus steeper than the non-corrected MF but still flatter than Salpeter's. For the innermost region, the fit to the completeness-corrected MF gives $\chi = 1.1 \pm 0.4$, which is the same slope derived for the intermediate region. Within uncertainties, the completeness-corrected MF slopes are uniform throughout the sampled region within the core, which suggests that we are not detecting significant differences in the mass segregation effects in such a small spatial scale, at least for stars more massive than $m \approx 1\,M_\odot$. It may be that a dynamical effect, such as mass segregation, cannot be detected given the relatively high stellar mass range covered by the present observations, basically $\gtrsim 1\,M_\odot$, and that deeper data (and lower masses stars) are needed to ascertain this issue. In any case, the relatively flat core MF derived in Fig. 13 suggests that dynamical effects have affected the core as a whole.

The total stellar mass in the core can be estimated by using the MF derived for the region 0.0 − 0.6 arcmin, and extrapolating it down to the H-burning mass limit, 0.08 $M_\odot$. This procedure may overestimate the total core stellar mass since it does not account for the evaporation of low-mass stars. Nevertheless, one can provide an upper limit estimate to the cluster mass. With the observed MFs, we derive an extrapolated stellar mass of 730 $M_\odot$. Since we are sampling ∼2/3 of the core radius, the (observed) core mass would be about 2000 $M_\odot$. Bonatto & Bica (2005) estimated that for Gyr-class OCs, in general, the extrapolated cluster mass is about 10 times that of the core. Thus, the total (observed and extrapolated) stellar mass of FSR 1415 would be about $2 \times 10^4\,M_\odot$, which is comparable to those of low-mass globular clusters (Harris 1996, and references therein).

When applying the same arguments to the completeness-corrected MF, the total (upper limit) cluster mass is estimated to be $\sim 3 \times 10^4\,M_\odot$, i.e. ∼50 per cent higher than the observed value. Once again, such a high-mass estimate can be accounted for by the facts that (i) the cluster is significantly more extended than the VLT/MAD-sampled region (Fig. 11) and (ii) the MFs were extrapolated down to 0.08 $M_\odot$ stars (while the observed mass range corresponds to stars more massive than $\approx 0.9\,M_\odot$). In any case, both mass estimates are consistent with the large core ($R_c \approx 2.6$ pc)

and tidal ($R_t \approx 35$ pc) radii. Overall, the above mass and radii estimates indicate a massive open cluster which shows evidence of an advanced dynamical state, given its relatively flat core MF. Thus, and in spite of being an outer massive disc cluster, FSR 1415 may present features of dynamical evolution, suggesting that it may have undergone significant encounters with GMCs and other tidal effects.

4 CONCLUDING REMARKS

The present study shows that the cluster candidate FSR 1415 (Froebrich, Scholz & Raftery 2007a) is confirmed as a genuine old open cluster. Thus, the Froebrich et al. catalogue appears to be an important source of interesting cluster candidates and is worthy of further examination.

The high-resolution and deep VLT/MAD *J* and *K* data of FSR 1415 have allowed an accurate determination of basic cluster parameters. It is of great importance to obtain similar high-quality data for other outer disc open clusters and complement these with spectroscopic metallicity determinations. Consequently, one can explore the age–metallicity–position dependencies all across the Galaxy. But perhaps first of all we need to overcome the current selection bias of old open clusters in the III and IV Galaxy quadrants.

ACKNOWLEDGMENTS

The anonymous referee is acknowledged for helpful suggestions. We thank the ESO Adaptive Optics group and in particular Enrico Marchetti and Paola Amico. We acknowledge partial financial support from the Brazilian agencies CNPq and FAPESP. SO acknowledges the Italian Ministero dell'Università e della Ricerca Scientifica e Tecnologica. YM wishes to thank Marco Gullieuszik and Simone Zaggia for useful discussions on the MAD performance.

REFERENCES

Ascenso J., Alves J., Vicente S., Lago M. T. V. T., 2007, A&A, 476, 199
Bica E., Bonatto C., Barbuy B., Ortolani S., 2006, A&A, 450, 105
Bonatto C., Bica E., 2005, A&A, 437, 483
Bonatto C., Bica E., 2006, A&A, 460, 83
Bonatto C., Bica E., 2007a, A&A, 473, 441
Bonatto C., Bica E., 2007b, A&A, 473, 445
Bonatto C., Bica E., 2008a, A&A, 477, 829
Bonatto C., Bica E., 2008b, A&A, 479, 741
Bonatto C., Bica E., Ortolani S., Barbuy B., 2006a, A&A, 453, 121
Bonatto C., Kerber L. O., Bica E., Santiago B. X., 2006b, A&A, 446, 121
Bonatto C., Bica E., Ortolani S., Barbuy B., 2007, MNRAS, 381, L35
Bouy H., Kolb J., Marchetti E., Martín E. L., Huélamo N., Barrado Y Navascués D., 2008, A&A, 477, 681
Bragaglia A.Sestito P., Villanova S., Carretta E., Randich S., Tosi M., 2008, A&A, 480, 79
de Marchi F., de Angeli F., Piotto G., Carraro G., Davies M. B., 2006, A&A, 459, 489
Drimmel R., Spergel D. N., 2001, ApJ, 556, 181
Dutra C. M., Santiago B. X., Bica E., 2002, A&A, 383, 219
Dutra C. M., Ortolani S., Bica E., Barbuy B., Zoccali M., Momany Y., 2003, A&A, 408, 127
Eisenhauer F. et al., 2005, ApJ, 628, 246
Elson R. A. W., Fall S. M., Freeman K. C., 1987, ApJ, 323, 54
Friel E. D., 1995, ARA&A, 33, 381
Friel E. D., Janes K. A., Tavarez M., Scott J., Katsanis R., Lotz J., Hong L., Miller N., 2002, AJ, 124, 2693
Froebrich D., Scholz A., Raftery C. L., 2007a, MNRAS, 374, 399
Froebrich D., Meusinger H., Scholz A., 2007b, MNRAS, 377, L54
Froebrich D., Meusinger H., Davis C. J., 2008, MNRAS, 383, L45
Girardi L., Bertelli G., Bressan A., Chiosi C., Groenewegen M. A. T., Marigo P., Salasnich B., Weiss A., 2002, A&A, 391, 195
Groenewegen M. A. T., Udalski A., Bono G., 2008, A&A, 481, 441
Gullieuszik M. et al., 2008, A&A, 483, L5
Harris W. E., 1996, AJ, 112, 1487
King I., 1962, AJ, 67, 471
King I., 1966, AJ, 71, 64
Lamers H. J. G. L. M., Gieles M., Bastian N., Baumgardt H., Kharchenko N. V., Portegies Zwart S., 2005, A&A, 441, 117
López-Corredoira M., Cabrera-Lavers A., Garzón F., Hammersley P. L., 2002, A&A, 394, 883
Maciel W. J., Quireza C., Costa R. D. D., 2007, A&A, 463, L13
Marchetti E., Brast R., Delabre B., Donaldson R., Fedrigo E., Frank C., Hubin N., Kolb J., 2007, The Messenger, 129, 8
Mermilliod J. C., 1996, in Milone E. F., Mermilliod J.-C., eds, ASP Conf. Ser. Vol. 90, The Origins, Evolution, and Destinies of Binary Stars in Clusters. Astron. Soc. Pac., San Francisco, p. 475
Momany Y., Held E. V., Saviane I., Rizzi L., 2002, A&A, 384, 393
Momany Y. et al., 2003, A&A, 402, 607
Momany Y., Zaggia S., Bonifacio P., Piotto G., De Angeli F., Bedin L., Carraro G., 2004, A&A, 421, L29
Momany Y. et al., 2005, A&A, 439, 111
Momany Y., Zaggia S., Gilmore G., Piotto,,Carraro G., Bedin L., de Angeli F., 2006, A&A, 451, 515
Momany Y., Held E., Saviane I., Zaggia S., Rizzi L., Gullieuszik M., 2007, A&A, 468, 973
Nishiyama S. et al., 2006, ApJ, 647, 1093
Pavani D. N., Bica E., 2007, MNRAS, 468, 139
Reid N., 1993, ARA&A, 31, 345
Robin A. C., Reylé C., Derrière S., Picaud S., 2003, A&A, 409, 523
Rocha-Pinto H. J., Rangel R. H. O., Porto de Mello G. F., Bragança G. A., Maciel W. J., 2006, A&A, 453, L9
Salaris M., Weiss A., Percival S. M., 2004, A&A, 422, 217
Salpeter E., 1955, ApJ, 121, 161
Stetson P. B., 1994, PASP, 106, 250
Trager S. C., King I. R., Djorgovski S., 1995, AJ, 109, 218
Upgren A. R., Mesrobian W. S., Kerridge S. J., 1972, AJ, 77, 74
Vallée J. P., 2008, AJ, 135, 1301
Venn K. A., Irwin M., Shetrone M. D., Christopher T., Hill V., Tolstoy E., 2004, AJ, 128, 1177
Wilson C. P., 1975, AJ, 80, 175
Yong D., Carney B. W., Teixeira de Almeida M. L., 2005, AJ, 130, 597

This paper has been typeset from a TEX/LATEX file prepared by the author.